Soils and Rocks
An International Journal of Geotechnical and Geoenvironmental Engineering
www.soilsandrocks.com
ISSN 1980-9743
ISSN-e 2675-5475

A novel stiffened deep soil mixing wall system for deep excavations in soft clay: 3D numerical analysis

Amira Aissaoui[1], Rafik Boufarh[2#], Farid Boursas[2], Adel Djellali[3]

Article

Keywords
Deep excavation
Soft soil
Stiffened Deep Soil Mixing
Connectors
Lateral displacement
Settlement

Abstract

Deep excavations in soft soils present complex geotechnical challenges, particularly in maintaining stability during the construction process. The low shear strength and high compressibility of these soils often lead to failure mechanisms that require careful analysis. This study introduces a novel Stiffened Deep Soil Mixing retaining wall system with connectors (SDSMC) for deep excavations in soft clay. Using 3D finite element analysis, the performance of the SDSMC wall was evaluated under varying steel column profile orientations, profile sizes (HEA 100, 200, and 300), and connector configurations. Results show 66% reduction in lateral displacement and 64% reduction in ground settlement compared to conventional Deep Soil Mixing walls. Superior performance was achieved when the strong axis of the HEA (H-beam European standard, series A) section was oriented perpendicular to the lateral earth pressure (X-orientation) and with larger profiles (HEA 300). Strategic connector placement, particularly with two connectors positioned at the top and bottom of the steel column, enhanced wall performance by up to 30%. The findings validate the SDSMC system as a cost-effective, robust, and sustainable alternative for urban deep excavations in soft clay conditions, further experimental validation is recommended to confirm its performance under realistic field conditions and to account for factors such as interface behavior, construction tolerances, and long-term soil-structure interaction.

1. Introduction

Global urbanization continues to drive complex infrastructure development within densely populated areas, leading to an increase in deep excavation projects under challenging geotechnical conditions, particularly in soft clay soils (Bozkurt et al., 2023; Do et al., 2016; Liu et al., 2011; Su et al., 1998). These soils exhibit low shear strength and high compressibility, creating significant challenges for excavation stability and adjacent structure safety. Traditional support systems, such as diaphragm walls and anchored sheet piles, are expensive, time-consuming, and environmentally disruptive (Ou, 2014; Yan et al., 2025). Consequently, there is a pressing need for innovative, efficient, and sustainable solutions to enhance deep excavation stability in soft clay conditions. Deep Soil Mixing (DSM) and its variant Stiffened Deep Soil Mixing (SDSM), represent promising alternatives. The effectiveness of these techniques has been demonstrated in numerous published works (Andromalos & Bahner, 2003; Jamsawang et al., 2016; Mun et al., 2012; Topolnicki, 2004; Waichita et al., 2019). This in-situ method employs binders to stabilize weak soils, thereby significantly augmenting their bearing capacity, stability, and settlement behavior. Both the technique and specific binder composition are crucial in optimizing the performance of treated soils (Gupta & Kumar, 2023; Bruce, 2000; Hessouh et al., 2023). Notably, in soft clay deposits, this technique has proven effective in improving soil properties for foundation support, embankment and slope stabilization, and seismic liquefaction mitigation (Chen et al., 2013; López Ramírez et al., 2024; Bouassida et al., 2022; Navin, 2005). Despite its numerous advantages in various applications, DSM can fail and collapse, particularly under lateral loading. Moreover, the DSM walls, due to their low tensile strength, require substantial cross-sectional thickness and are typically constructed without strut support (Wang et al., 2010). These characteristics can render DSM walls impractical for urban deep excavations, where space is often constrained. In response to the flexural capacity limitations and unexpected failures of DSM walls, engineers developed Stiffened Deep Soil Mixing (SDSM) walls as an effective alternative retention system for deep excavations in soft clay conditions. This modification incorporates a rigid core to increase soil stiffness. The process involves inserting a prefabricated pile into the center of a deep mixed column after

#Corresponding author. E-mail address: rafik.boufarh@univ-tebessa.dz
[1]Echahid Cheikh Larbi Tebessi University, Department of Civil Engineering, Mining Laboratory, Tebessa, Algeria.
[2]Echahid Cheikh Larbi Tebessi University, Department of Civil Engineering, Laboratory of Applied Civil Engineering, Tebessa, Algeria.
[3]Echahid Cheikh Larbi Tebessi University, Mining Institute, Environmental Laboratory, Tebessa, Algeria.

Submitted on January 8, 2025; Final Acceptance on September 25, 2025; Discussion open until May 31, 2026.

Editor: Renato P. Cunha

https://doi.org/10.28927/SR.2026.000325

mixing soil with injected cement, while the cemented soil is still in its early curing stage. Over the past decades, numerous studies have been conducted to evaluate the performance of SDSM columns using various analytical and experimental methods. Voottipruex et al. (2011) investigated the behavior and performance of two types of ground improvement techniques: conventional DSM columns and SDSM columns under full-scale loading conditions. Through experimental tests and numerical simulations, the researchers analyzed the bearing capacity, settlements, stress distribution, and failure mechanisms of these two column types. The results demonstrated the superiority of SDSM columns compared to conventional DSM columns, particularly in terms of higher bearing capacity, reduced settlements, and better structural integrity. Raongjant & Jing (2013) investigated the performance of SDSM piles under lateral cyclic loading through field testing. They constructed and tested three SDSM piles with different types of stiffer cores (H-shaped cross-section, steel pipe, and H-column steel), subjecting them to cyclic lateral loading and monitoring their displacement and strain. Test results showed that SDSM piles with H-column steel cores achieved lateral carrying capacities 3-4 times higher than conventional DSM piles. Field observations confirmed the effectiveness of SDSM piles for mitigating lateral loads in seismic zones, with H-column steel reinforcement further enhancing their performance under cyclic loading conditions. In their study, Wonglert et al. (2018) examined the performance of floating SDSM columns subjected to axial loading conditions. This study focused on the bearing capacity characteristics, failure mechanisms, and load transfer behavior of these floating columns, which combine cement mixing with core reinforcement but do not extend to a firm bearing stratum. Through experimental testing and detailed analysis, the researchers examined the influence of column length, soil conditions, and the strength of the DSM socket on the load-bearing capacity and failure modes of the columns. The experimental findings demonstrated that pile materials possessing lower strength and stiffness characteristics, such as eucalyptus wood, could be viable options for reinforced pile cores. Zhang et al. (2020) developed a design method for calculating settlements of embankments supported by SDSM columns in soft clay soils. Their research presents a comprehensive theoretical framework that addresses load transfer mechanisms, soil-structure interaction, and settlement components. Through field measurement validation, they investigated settlement mechanisms, load distribution patterns, and the influence of soft clay properties on system performance. The proposed method incorporates settlement components, stress distribution patterns, and time-dependent behavior, providing practical design procedures. This study advanced geotechnical engineering practice by offering reliable settlement prediction tools for SDSM column-supported embankments on soft clay foundations. Phutthananon et al. (2023) focused on evaluating the reliability of embankments supported by SDSM columns, specifically concerning their serviceability limit states. They developed probabilistic models to assess the variability of soil and SDSM column properties, the impact of different design parameters, and the reliability of the system under different conditions. Using advanced numerical methods including finite element analysis, reliability assessment techniques, and statistical analysis of performance data, the study provided reliability indices for different design scenarios and guidelines for serviceability-based design.

Based on insights from previous research, this study addresses these limitations by introducing a novel SDSM wall system with connectors (SDSMC), which enhances lateral resistance and minimizes ground settlement. The connectors improve the composite action between the steel column and DSM column, offering a more efficient and sustainable solution for deep excavations in soft clay. Utilizing advanced three-dimensional finite element analysis, a comprehensive parametric study was conducted on key design parameters. HEA (H-beam European standard, series A) steel column profiles have higher I_y (strong axis, perpendicular to the flanges) and lower I_z (weak axis, parallel to the flanges). X-orientation places the strong axis of the HEA section perpendicular to the direction of the lateral earth pressure, while Y-orientation positions the weak axis of the HEA section parallel to the direction of the lateral earth pressure. This investigation examined steel profile orientation (X-direction, Y-direction, and inclined I-direction), profile sizes (HEA 100, HEA 200, and HEA 300), and connector configurations to optimize control of lateral displacement and ground settlement. The 3D finite element model captures complex interactions that simpler approaches cannot address, including lateral earth pressure redistribution, wall bending in multiple directions, and the combined effects of soil stratification and construction sequencing. These phenomena cannot be adequately represented by simplified analytical formulations or 2D analysis. The numerical analyses employed both the Hardening Soil model and the Soft Soil Creep model to simulate soft clay behavior and predict short-term performance while optimizing construction sequences—a critical aspect inadequately explored in existing literature.

2. Problem definition

Excavation works in soft clay exhibit undrained creep behavior, which causes lateral movements of the excavated slopes over time. A study by Voottipruex et al. (2019) revealed that applied stress levels significantly impact the rates of lateral movements observed in excavated slopes. The research showed that SDSM columns offered substantially higher ultimate lateral load capacity and ductility compared to conventional DSM columns. Increasing the friction between the DSM column and the steel column within the SDSM system represents one potential approach to improving the lateral load transfer mechanism. The new SDSMC design, incorporating stiffer H-column steel connectors and cores,

aims to enhance lateral resistance while minimizing ground settlement behind retaining walls. The strategic positioning of connectors along the steel column could enhance the composite action between the steel and DSM column. Each connector in the SDSMC wall serves specific purposes based on its vertical position. This highlights the importance of enhancing the lateral load resistance and ductility of DSM columns, especially in soft clay conditions where creep and lateral movements are prevalent.

3. Numerical analysis

3.1 Model geometry and mesh size

This study examines the response of Stiffened Deep Soil Mixing walls with connectors (SDSMC) to deep excavation using Plaxis 3D Version 2020, a widely recognized finite element software for geotechnical applications. The numerical model was developed to simulate the excavation process and the behavior of the SDSMC wall under varying conditions. The 3D finite element model was designed to replicate a typical deep excavation scenario in soft clay. The model dimensions were 30 m in width, 60 m in length, and 16 m in depth, representing a realistic excavation site. Figure 1 illustrates the model geometry used in the study.

The SDSMC wall was positioned at the center of the model, with the steel H-column embedded within the DSM column. The groundwater level was assumed to be at the surface, typical for Bangkok soft clay conditions (Voottipruex et al., 2019). Suction stresses were not modeled, as the analysis focuses on short-term behavior in saturated soil. The cross-sectional arrangement of the DSM and SDSM wall is presented in Figure 2, showing the embedded steel H-columns. The connectors were added to each side of the steel column, placed at different depths along the upper surface, in the middle of the column, and on the lower surface. Various connector positions in the SDSMC wall are shown in Figure 2.

The model was discretized using a structured mesh with an average element size of 0.5 m. This mesh size was selected to balance computational efficiency and accuracy.

A finer mesh (0.25 m) was applied near the SDSMC wall and excavation area to capture localized deformations and stress concentrations, while a coarser mesh (1.0 m) was used in regions farther from the excavation to reduce computational cost. The mesh consisted of 10-node tetrahedral

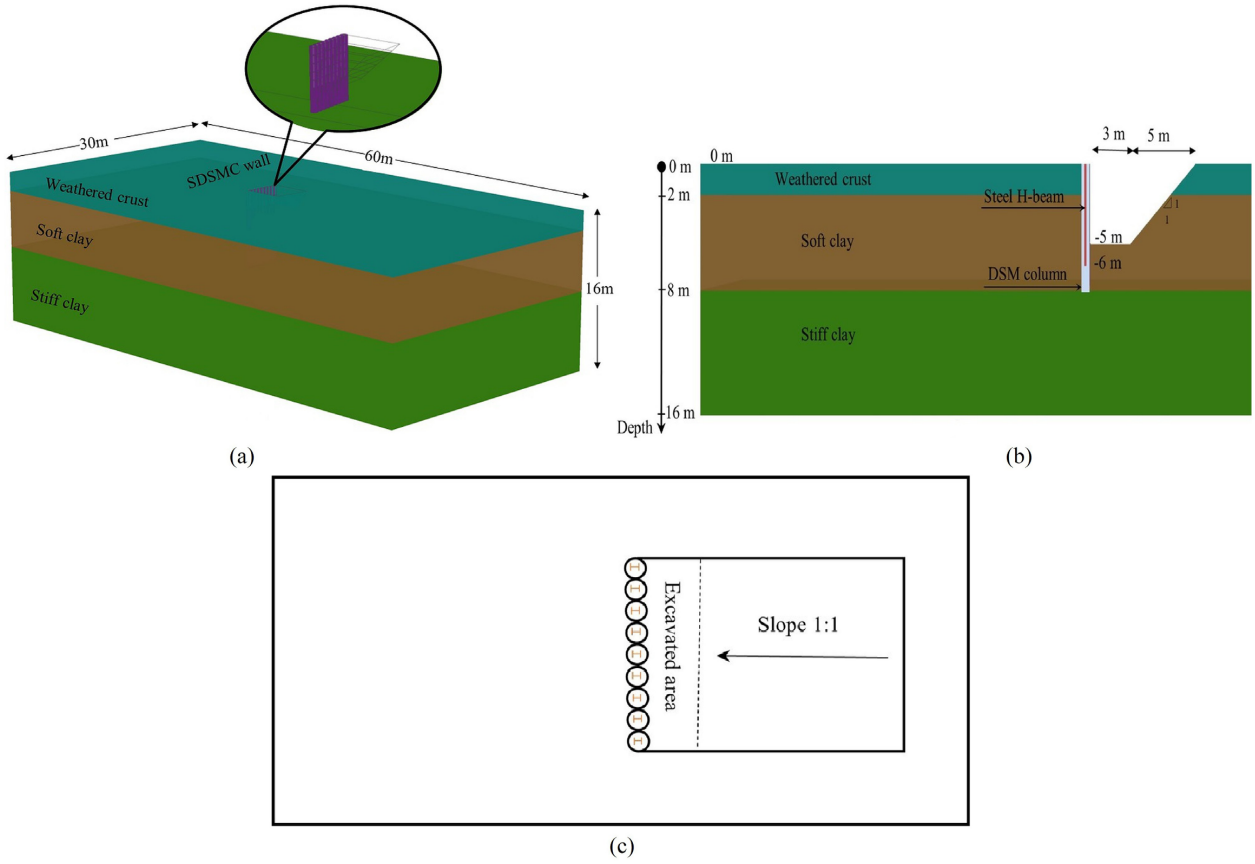

Figure 1. Model geometry: (a) 3D view of the soil profile and SDSMC wall; (b) cross-sectional view of the soil profile, steel H-column, and DSM column; (c) Plan view.

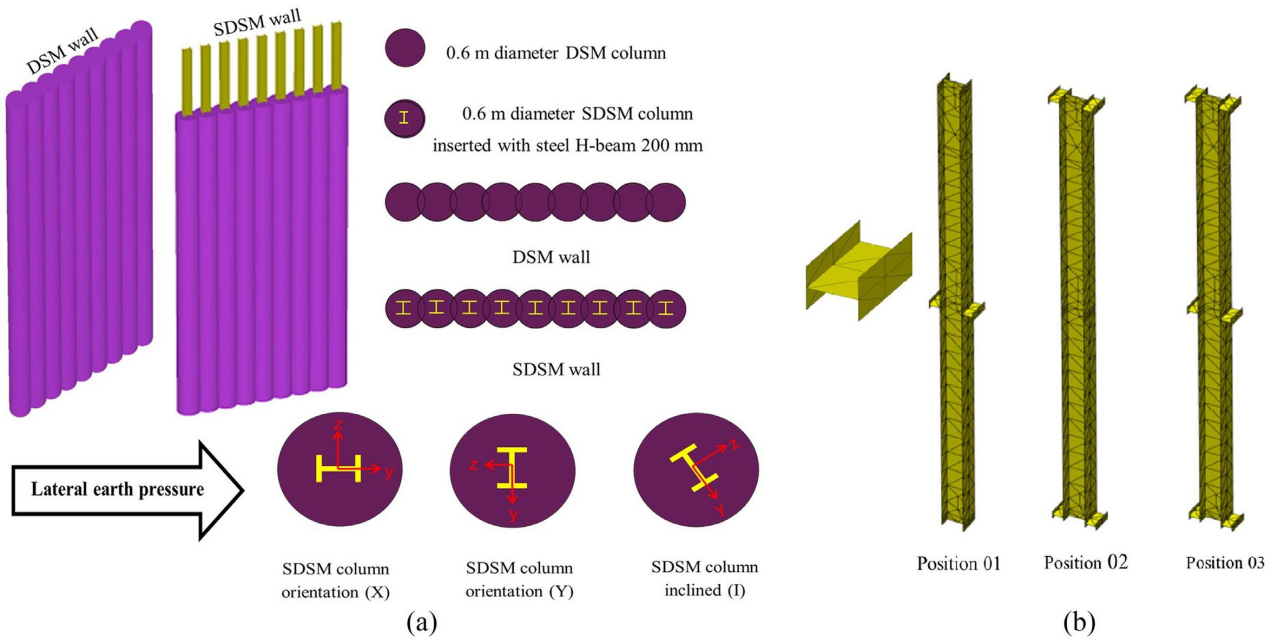

Figure 2. (a) Schematic illustration of the DSM wall and SDSM wall and (b) Schematic illustration of the Steel H-column with connector positions in the structure.

elements for the soil and 6-node plate elements for the steel H-column and connectors as see in Figure 3.

3.2 Boundary conditions

The boundary conditions were carefully defined to replicate real-world constraints and ensure accurate simulation results. The sides of the model were fixed in the horizontal direction (X and Y) to prevent lateral movement, simulating the presence of adjacent soil masses. The bottom boundary was fixed in all directions (X, Y, and Z) to represent the rigid bedrock layer underlying the soil profile. The ground surface was left free to move in all directions, allowing for realistic settlement and deformation patterns during excavation. The excavation process was simulated in stages, with each stage representing a 1-meter depth increment. At each stage, the soil elements within the excavation zone were deactivated, and the corresponding stresses were redistributed to the remaining soil mass. The steel column-DSM column interface was modeled with full bonding (no slip) (Voottipruex et al., 2019).

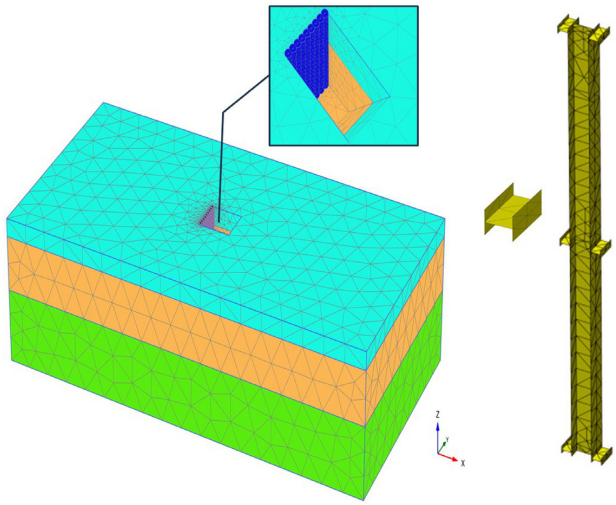

Figure 3. Three-dimensional finite element mesh model of deep excavation with SDSM wall system.

3.3 Constitutive model and materials parameters

The foundation soil profile was taken from full-scale experiments conducted in Bangkok, Thailand, by Voottipruex et al. (2019). At this site, the soil profile consisted of a 2 m thick weathered crust, a 6 m thick extremely soft to soft clay layer, an 8 m thick stiff clay layer, and an underlying layer of thick, compact sand. Figure 1b depicts the stratification of the foundation soil profile. Table 1 summarizes the material characteristics of the DSM columns and the foundation soil. The Hardening Soil (HS) constitutive model was employed to simulate the behavior of the DSM columns, stiff clay, and weathered crust layers. This model accounts for the nonlinear stress-strain behavior of soils, considering crucial factors like stress history and soil hardening/softening. These factors are essential in the deformation response of soils during excavation processes. One of the key advantages of the HS model is its ability to capture the stress-dependent stiffness

Table 1. Material parameters for the Hardening Soil Model (HS) used for weathered crust, stiff clay, and DSM columns (Voottipruex et al., 2019).

Parameters	Weathered crust	Stiff clay	DSM column
Unit weight, γ (KN/m³)	17	20	16
Secant stiffness, E_{50}^{ref} (MPa)	17	20	35
Tangential stiffness, E_{oed}^{ref} (MPa)	13	25	35
Unloading and reloading stiffness, E_{ur}^{ref} (MPa)	62	95	240
Power of the stress-level dependency of the stiffness, m	1	0.9	0.4
Poisson's ratio for unloading-reloading, v_u	0.2	0.2	0.2
Cohesion, c' (kPa)	15	30	350
Friction angle, φ' (degree)	27	23	40

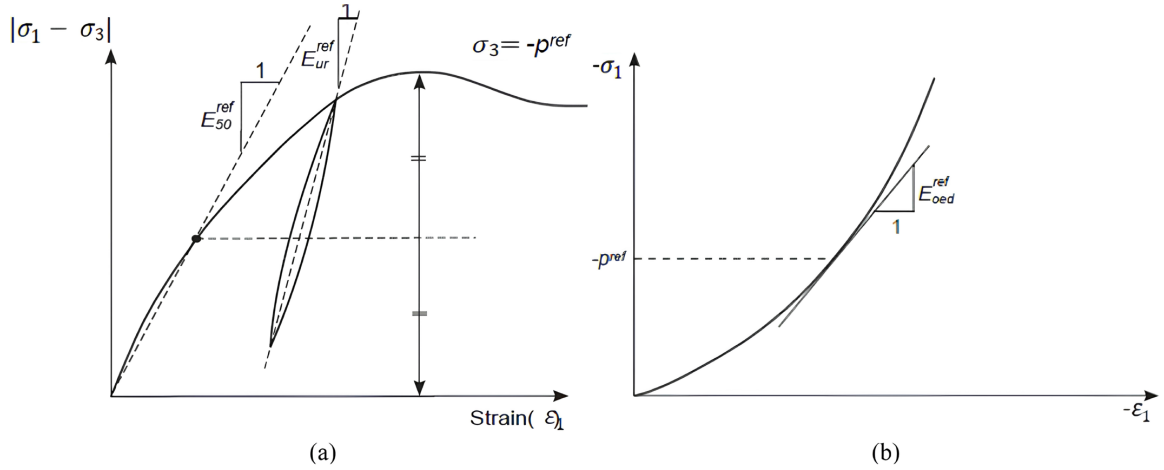

Figure 4. Illustration of reference Stiffness Moduli for (a) Triaxial Tests (b) oedometer tests results.

of soils, which is governed by a power law relationship. As the stress state within the soil changes during excavation stages, the model can accurately represent the corresponding variations in soil stiffness, leading to more reliable predictions of soil deformations (Schanz et al., 2019). Additionally, the HS model incorporates parameters related to plastic straining due to primary deviatoric loading and primary compression, as well as elastic unloading/reloading behavior. The stiffness of the soil varies with the stress level according to the following equation:

$$E = E_{ref} * \left(\sigma_3' / \sigma_{ref}\right)^m \quad (1)$$

where: E is the soil stiffness, E_{ref} is a reference stiffness at a reference stress (σ_{ref}), σ_3' is the current confining stress, m is the power law exponent ($0 \leq m \leq 1$). A value of $m = 1$ represents a soil with constant stiffness, while $m = 0$ represents an infinitely hardening soil.

As shown in Figure 4, which illustrate the reference Stiffness Moduli. The plastic straining due to primary deviatoric loading E_{50}^{ref} represents the secant stiffness in triaxial compression at 50% of the confining stress and controls the level of plastic strain in the soil under primary deviatoric loading. The plastic straining due to primary compression E_{oed}^{ref} is the reference oedometric modulus, i.e., the stiffness for a primary oedometric stress path at the reference stress.

Elastic unloading/reloading (input parameters E_{ur}^{ref}, v_{ur}): E_{ur}^{ref} and v_{ur} govern the unloading/reloading stiffness of the soil and its Poisson's ratio for elastic deformations, respectively.

An undrained analysis was performed for the soft clay layers using the Soft Soil Creep model, to reflect the short-term behavior during excavation. The soft soil creep model is a specialized constitutive model designed to understand the time-dependent behavior of soft soils under sustained loads. Derived from the modified Cam-clay model, it incorporates additional parameters to account for creep, the gradual accumulation of deformations over time under constant effective stress. Under this assumption, stiffness and strength are defined in terms of effective properties (φ' and c'). A large bulk stiffness for water is automatically applied to make the soil as a whole incompressible, and (excess) pore pressures are calculated, even above the phreatic surface clay (Brinkgreve, 2004; Vermeer & Neher, 1999). This approach is crucial for predicting soil behavior and potential settlements, which can significantly impact

the serviceability of structures founded on soft. The specific parameters for this model are detailed in Table 2. The soft soil creep model's basic parameters encompass several key aspects that describe the mechanical behavior of soil under various loading conditions. The modified compression index (λ^*) represents a fundamental parameter defined by the slope of the normal compression line in the void ratio-logarithmic effective plane. This parameter quantifies soil compressibility under virgin loading conditions and serves as a critical input for settlement predictions under imposed stress states. The modified compression index is calculated as $\lambda^* = \lambda / (1+e_0)$, where λ is the compression index, and e_0 is the initial void ratio of the soil.

Complementing the compression index, the modified swelling index (k^*) characterizes soil response during unloading-reloading cycles. This parameter is essential for analyzing structures subjected to cyclic or fluctuating stress conditions, as it defines the slope of the unloading-reloading line in the void ratio-logarithmic effective stress plane. The modified swelling index is calculated as $k^* = k / (1+e_0)$, where k is the swelling index. The modified creep index (μ^*) constitutes the distinctive parameter of the soft soil creep model. This parameter quantifies time-dependent viscous deformations occurring in soft soils under sustained loading conditions. The modified creep index is calculated as $\mu^* = \mu / (1+e_0)$, where μ represents the conventional creep index. Through this formulation, the model effectively captures secondary compression phenomena and the progressive accumulation of time-dependent strains, which is a critical mechanism governing long-term settlement behavior of cohesive soils (Brinkgreve, 2004; Vermeer & Neher, 1999).

Table 2. Soft soil creep model parameters for soft clay characterization (Voottipruex et al., 2019).

Parameters	Soft clay
Unit weight, γ (kN/m³)	15
Modified compression index, λ^*	0.076
Modified swelling index, k^*	0.028
Modified creep index, μ^*	0.007
Poisson's ratio for unloading-reloading, ν_{ur}	0.15
Cohesion, c' (kPa)	2
Friction angle, φ' (degree)	23

The steel H-column was modeled using columns elements, and the material properties assigned to the connectors were identical to those of the steel column. Table 3 shows all the properties related to this model.

4. Results and discussions

To ensure the accuracy of the numerical model for this study, a validation process was undertaken using data from lateral load tests conducted by Voottipruex et al. (2019). The numerical model was validated against two configurations from their study: (1) a 0.6 m diameter, 8 m deep DSM column used for soil reinforcement, and (2) an SDSM column of the same dimensions supporting a 6 m steel H-column capped with a 1 m thick concrete cap. The lateral load-displacement response for these configurations is shown in Figure 5. The close agreement between experimental and simulated results demonstrates the robustness and accuracy of the finite element model, establishing its value for designing and analyzing DSM and SDSM walls in similar soil conditions.

After completing the verification process, we will present selected results in the following figures.

The left side of Figure 6 shows deformation vectors concentrated near the SDSMC wall, particularly at the top,

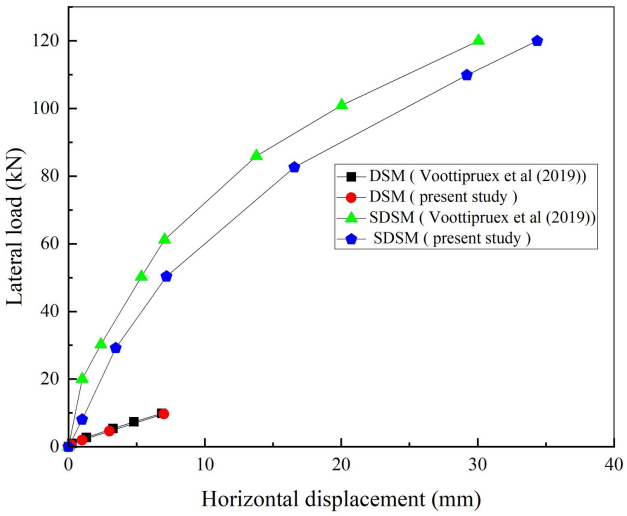

Figure 5. Results comparisons of the present study with the previous study by Voottipruex et al. (2019).

Table 3. Material properties of the steel H-column.

Parameters	HEA 100	HEA 200	HEA 300
Material type	Elastic	Elastic	Elastic
Unit weight, γ (kN/m³)	78.50	78.50	78.50
Cross section (cm²)	21.20	53.80	113
Moment of Inertia Iy (cm⁴)	349	3690	18260
Moment of Inertia Iz (cm⁴)	134	1340	6310
Young's modulus (kN/m²)	210x10⁶	210x10⁶	210x10⁶

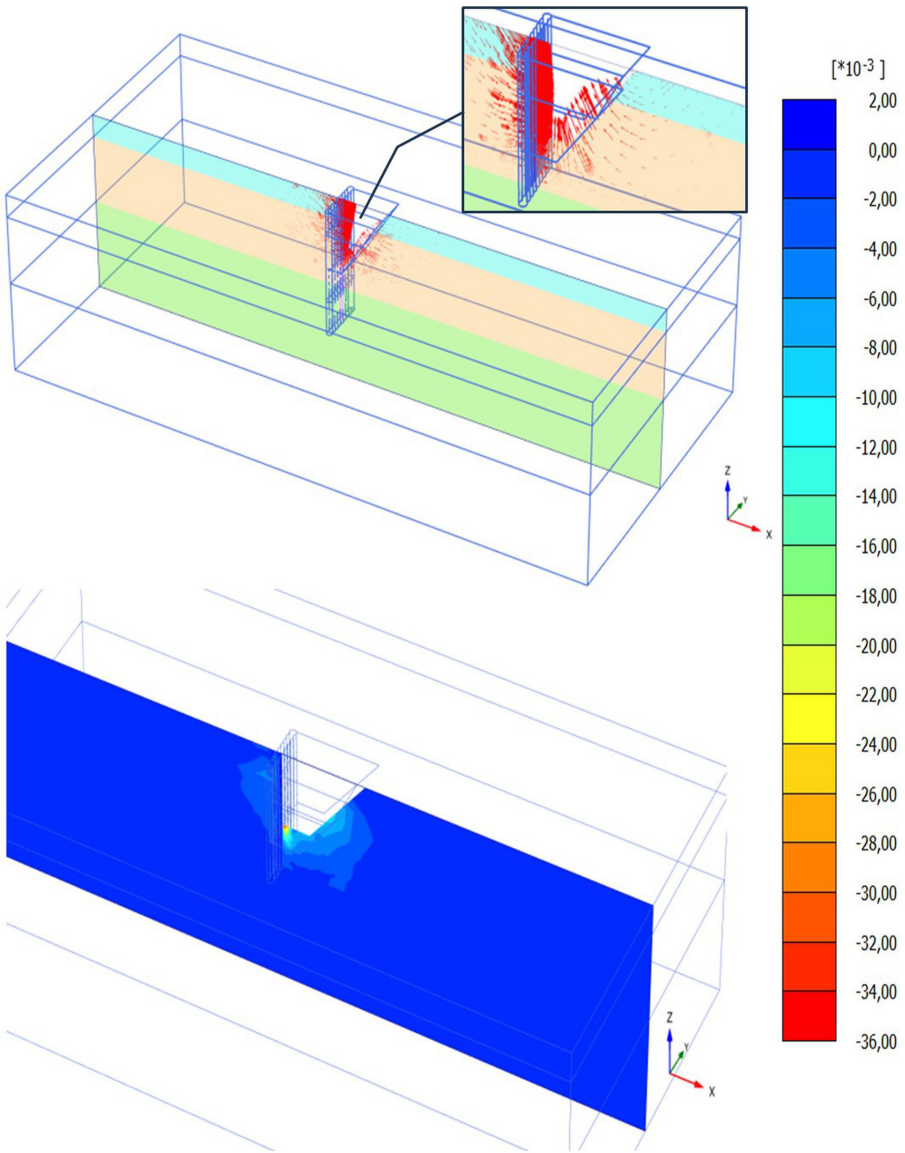

Figure 6. 3D finite element analysis results of deformation vectors and principal strains after final excavation.

extending into the retained soil mass (magnified inset). The vector directions indicate the typical soil movement pattern in deep excavations: primarily horizontal displacement of the wall with some rotation, and settlement of the retained soil behind the wall. The color gradation in the soil layers represents varying levels of strain or displacement magnitude across different soil strata.

The right side displays a principal strain contour plot with a blue-to-red color scale, indicating strain magnitudes ranging from minimum (blue) at approximately -0.02077 to maximum (red) at approximately 0.3391×10^{-2}, as noted in the legend box. The highest strain concentrations (red/orange areas) appear at the base of the excavation and behind the retaining wall, which is consistent with expected behavior in deep excavations where the maximum lateral wall displacement typically occurs at some depth below the excavation surface. The 3D visualization effectively captures the spatial distribution of strains throughout the entire model domain, demonstrating the advantage of three-dimensional analysis for capturing complex soil-structure interaction in excavation projects.

4.1 Steel profile orientation effect

HEA profiles have higher I_y (strong axis, perpendicular to the flanges) and lower I_z (weak axis, parallel to the flanges). X-orientation places the strong axis of the HEA section perpendicular to the direction of the lateral earth pressure, while Y-orientation positions the weak axis of the HEA section

parallel to the direction of the lateral earth pressure. Figure 7 presents a comparison of the lateral displacement profiles of different walls after excavation. These walls include various orientations of HEA 200 columns in both a Stiffened Deep Soil Mixing (SDSM) wall and a conventional DSM wall. The presence of a 2 m thick weathered crust layer contributed to the development of a bulging inward profile in the excavation area due to lateral displacement. The non-linear deformation suggests a softer soil layer between 2-4 m depth, where the maximum displacements occur. The top 1-2 m shows relatively smaller displacements due to the presence of a weathered crust layer. The DSM wall exhibits the largest lateral displacement, particularly in the middle bulging area; the maximum displacement occurs at about 3 m depth, reaching nearly 50 mm.

For the SDSM (X), SDSM (Y), and SDSM (I) techniques, they show similar curved displacement profiles with decreasing maximum displacements in that order. Maximum displacements are approximately 17.9 mm, 20.4 mm, and 19.7 mm for SDSM (X), SDSM (Y), and SDSM (I), respectively. The variation in maximum lateral displacement between the three SDSM techniques is relatively small, with a difference of approximately 3 mm between SDSM (Y) and SDSM (X). This is because the HEA 200 design incorporates a constant thickness across both the web and flanges. Compared to IPN profiles, it may show a more pronounced variation. SDSM (X) gives the best performance in minimizing lateral displacement.

Figure 7 also includes comparative data from previous work by (Voottipruex et al., 2019) for both DSM and SDSM walls. The results demonstrate strong convergence between the current study and previously published findings, validating the reliability and consistency of our numerical models.

Figure 8 illustrates ground surface settlements behind retaining walls with varying DSM and SDSM profiles and orientations. The DSM wall exhibits the largest settlement, reaching a maximum of -28 mm approximately 2 m behind the wall.

The area of influence extends to about 10 m from the wall, beyond which settlements are negligible. The SDSM X wall demonstrates the smallest settlement at -13 mm, which is less than half of the DSM wall's maximum. This peak settlement occurs closer to the wall, around 2 m behind it. The influence zone of the SDSM walls is narrower, with settlements becoming negligible at approximately 10 m from the wall. The HEA 200 (X, Y, and I) orientations exhibit very similar settlement behavior.

Figure 9 depicts the maximum settlement observed at each excavation stage for a conventional DSM wall and an SDSM

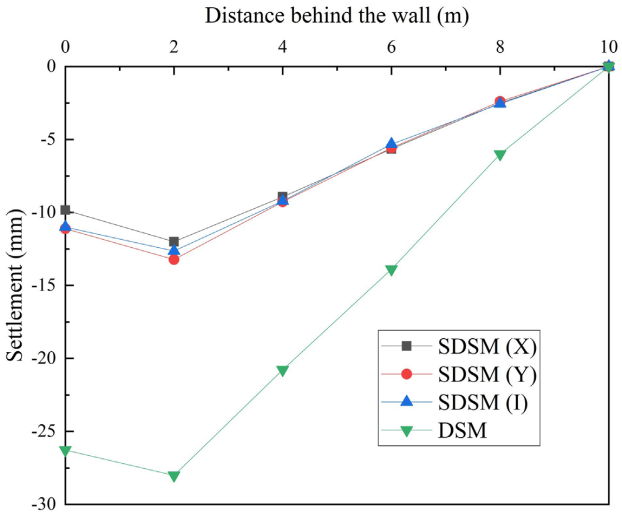

Figure 8. Settlement behind the wall for DSM and SDSM walls with different profile orientations (X, Y, and inclined I).

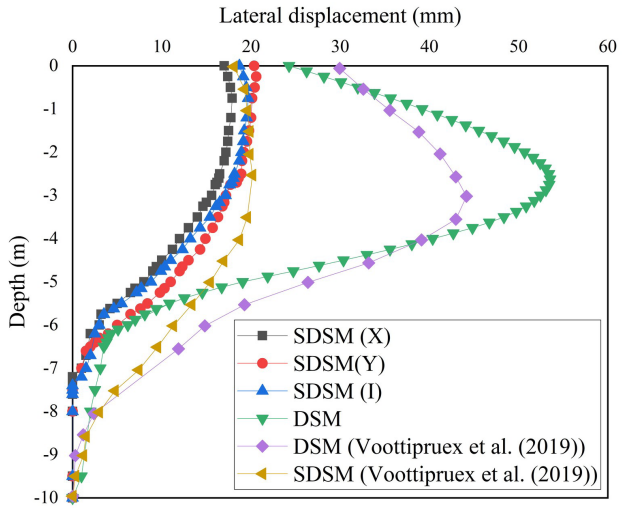

Figure 7. Lateral displacement as a function of depth for DSM and SDSM walls with three profile orientations (X, Y, and inclined I).

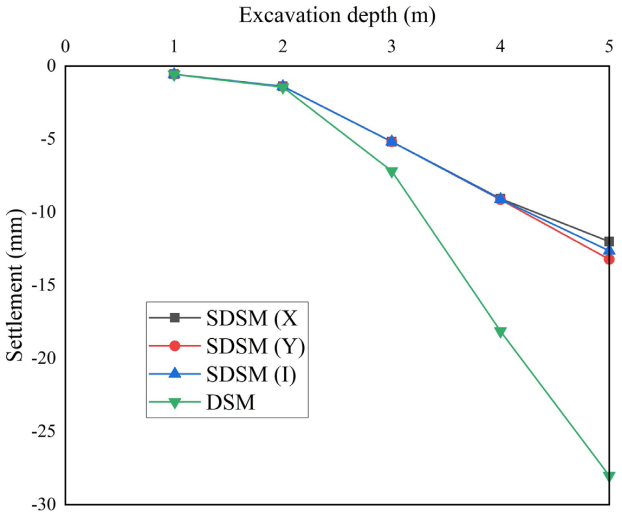

Figure 9. Maximum ground settlement progression across sequential excavation stages for DSM and SDSM walls with different profile orientations (X, Y, and inclined I).

wall with H-columns installed in various orientations. The graph presents settlement behavior at 1-meter excavation depth intervals up to a depth of 5 m. Notably, the rate of settlement increase is not linear with depth. A more pronounced increase in settlement is evident between 2 and 4 m of excavation depth. This accelerated settlement behavior can be attributed to the progressive redistribution of stresses within the remaining soil mass as the excavation deepens. As excavation progresses, the remaining soil mass experiences significant pressure redistribution. At final excavation depth, the soil has been subjected to prolonged periods of pressure, allowing for greater creep and settlement. Furthermore, deeper excavation exposes softer soil layers that are more susceptible to compression.

The observed settlement behavior can be explained by the soft soil creep model. This model posits that soil beneath the excavation undergoes time-dependent deformation under the sustained loading imposed by the excavation. Soil deformation typically occurs in three stages: immediate elastic deformation, primary consolidation, and secondary compression (creep). The increasing settlement with depth observed in the graph likely reflects a combination of these effects, with creep becoming increasingly significant at greater depths and over longer durations.

4.2 Profile type effect (HEA 100, 200 and 300)

Figure 10 compares the lateral displacement of DSM and SDSM walls with different core sections (HEA100, HEA200, and HEA300) with X-direction orientation. The conventional DSM wall exhibits the largest lateral displacements, with maximum values approaching 45 mm at approximately 4-5 m depth. This characteristic bulging deformation pattern is typical for flexible retaining walls in soft clay conditions. In contrast, all SDSM variants show significantly reduced lateral displacements, demonstrating the effectiveness of steel reinforcement in improving wall stiffness. Among the SDSM configurations, a clear correlation exists between HEA profile size and wall performance. The SDSM wall with HEA300 profiles demonstrates superior performance with lateral displacements limited to approximately 17 mm. The HEA200 configuration shows moderate performance with maximum displacements around 23.5 mm, while the HEA100 variant exhibits higher displacements of approximately 29.8 mm. This progressive improvement with increasing profile size confirms that the moment of inertia (I) of the steel reinforcement directly influences lateral wall stiffness. The results clearly demonstrate that incorporating larger steel profiles provides substantial benefits for controlling lateral deformations, with the HEA300 configuration reducing maximum displacement by approximately 66% compared to conventional DSM walls.

The ground surface settlement behind the wall is illustrated in Figure 11 for both DSM and SDSM walls, each spaced 2 m apart. The figure compares settlements for walls reinforced with HEA steel profiles of varying core sizes (HEA100, HEA200, and HEA300). The settlement

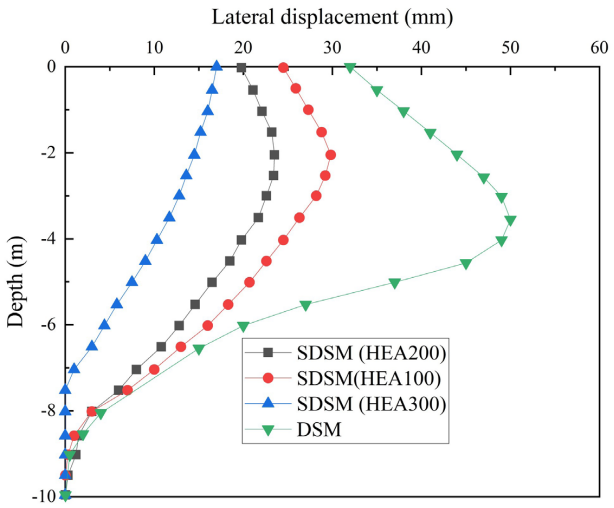

Figure 10. Lateral displacement as a function of for DSM and SDSM walls with different HEA profile sizes (100, 200, and 300).

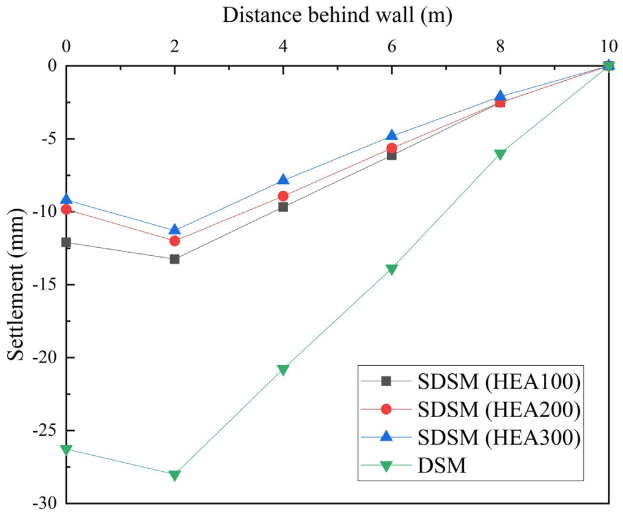

Figure 11. Settlement behind the wall for DSM and SDSM walls with different HEA profile sizes (100, 200, and 300).

curves for all SDSM configurations and DSM walls follow a similar trend, with maximum settlement occurring 2-3 m behind the wall and gradually decreasing thereafter.

The influence of the wall extends to approximately 8-10 m. SDSM walls demonstrate significantly better performance than DSM walls in controlling ground settlement, reducing maximum settlements by 57-64%. Specifically, the DSM wall settles by 28 mm, while SDSM walls with HEA100, HEA200, and HEA300 profiles settle by 12 mm, 11 mm, and 10 mm, respectively.

4.3 Connector effect

Figure 12 presents a comparison of lateral displacement profiles for SDSM walls with and without connectors (SDSMC)

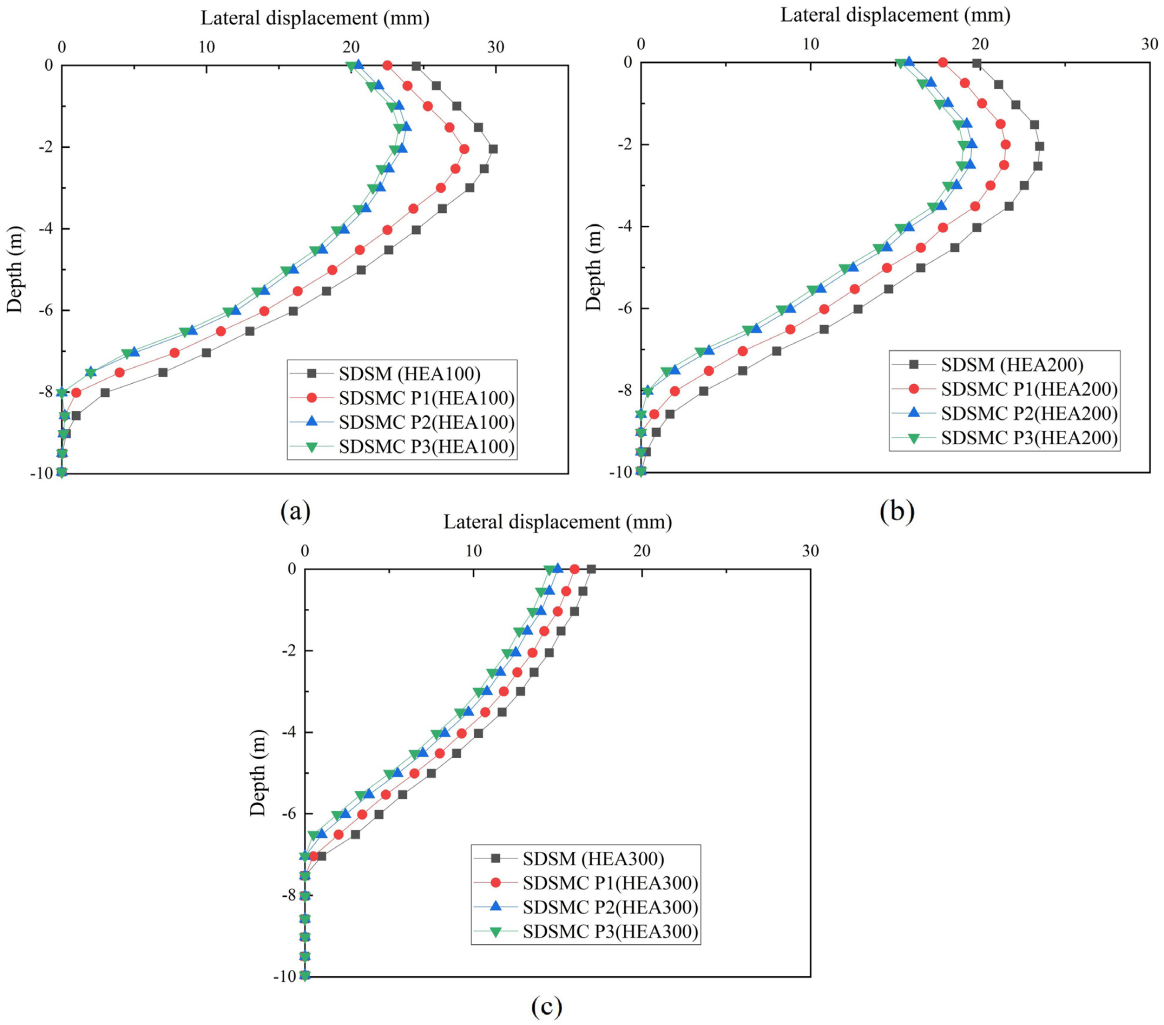

Figure 12. Lateral displacement profiles as a function of depth for SDSM and SDSMC retaining walls with varying HEA section sizes and connector positions (P1, P2, and P3): (a) HEA100; (b) HEA200; (c) HEA300.

across different HEA profile sizes (100, 200, and 300) and connector positions (P1, P2, and P3).

The results reveal that connector positioning significantly influences wall deformation behavior and demonstrates a clear correlation between HEA profile size and the effectiveness of lateral displacement control. Conventional SDSM walls exhibit the largest displacements, while the inclusion of connectors reduces lateral movement to varying degrees. Connector position P2 consistently demonstrates superior performance, achieving surface displacement reductions of 25-30% for HEA100, 20-25% for HEA200, and 9.2% for HEA300 compared to conventional SDSM walls. This optimal performance stems from P2's strategic positioning at the critical stress transfer zone, maximizing composite action between the steel H-profile and cemented soil matrix. The mechanical advantage derives from intercepting the primary lateral load path where maximum bending moments develop, transforming discrete elements into a unified composite structure through rigid mechanical interlock. Position P3 follows closely with reductions of 20-25% for HEA100, 15-20% for HEA200, and 11% for HEA300, while P1 demonstrates least effectiveness (15-20% for HEA100, 10-15% for HEA200, minimal 2% for HEA300). This performance hierarchy reflects positioning relative to the critical stress concentration zone and optimal bending moment region. In all configurations, the most significant improvements are concentrated within the top 4 m of the wall. Positions P2 and P3 provide the greatest stability near the surface, suggesting that adding a third connector does not offer additional benefits compared to using two connectors. Therefore, two connectors are sufficient to achieve optimal results. The effectiveness of the connectors diminishes with depth, converging to a 10-15% reduction for HEA100 and 5-10% for HEA200 at maximum depth.

The relationship between HEA section size and connector effectiveness reveals important mechanistic insights. Smaller

sections (HEA100) show greatest sensitivity to connector positioning due to inherently lower flexural rigidity, relying more heavily on composite behavior for lateral resistance. Conversely, larger sections (HEA300) demonstrate reduced sensitivity due to substantial inherent structural rigidity, which already provides effective lateral resistance independent of composite action.

The diminishing returns with HEA300 sections highlight that conventional SDSM walls with larger sections are already highly effective, making connector benefits marginal. This suggests connector implementation is most cost-effective for smaller steel sections where composite action provides greatest performance enhancement. Optimal connector design must therefore consider both steel section properties and stress distribution patterns to maximize composite behavior benefits.

Maximum lateral displacement patterns of SDSM and SDSMC walls are demonstrated in Figure 13, examining variations across HEA profiles (HEA100, HEA200, and HEA300) and connector positions (P1, P2, and P3).

The reduction in lateral displacement exhibits non-linear behavior, indicating that increasing the profile size from HEA100 to HEA200 with connectors provides a more significant improvement in lateral stiffness compared to increasing from HEA200 to HEA300.

HEA100 profiles show higher overall percentage reductions in displacement, suggesting that connector positioning has a more pronounced effect on smaller profiles, likely due to their inherent flexibility.

The analysis of lateral displacement reductions and percentage improvements between SDSM and SDSMC P2 configurations for HEA100 and HEA200 profiles reveals superior performance in HEA100 applications. Specifically, lateral displacement reductions for HEA100 range from 10% to 26%, while HEA200 shows reductions of 10% to 17%. Overall, the SDSMC P2 configuration achieves a 10-22% reduction in lateral displacement, demonstrating that the connector in position 2 significantly enhances the stiffness of the deep soil mixing wall. This improvement is particularly pronounced for smaller HEA profiles, such as HEA100, due to their inherent flexibility.

Figure 14 compares the maximum settlement behavior of SDSM and SDSMC walls using HEA 100, HEA 200, and HEA 300 profiles, considering different connector positions (P1, P2, and P3). The results indicate that both the size of the HEA profile and the connector position significantly influence settlement performance. For the HEA 100 profile, which exhibits the highest settlement values, the conventional SDSM configuration shows a settlement of approximately 13.5 mm. This value progressively decreases through connector positions P1 (12.5 mm), P2 (12 mm), and P3 (11 mm), representing improvements of 7.4%, 11.1%, and 18.5%, respectively. The HEA 200 profile demonstrates moderate settlement values, starting at 12 mm for the conventional SDSM configuration and decreasing to 11 mm (P1), 10 mm (P2), and 9.5 mm (P3), achieving reductions of 8.3%, 16.7%, and 20.8%, respectively. The HEA 300 configuration shows the lowest overall settlement values, beginning at 11.5 mm for the standard SDSM configuration and reducing to 10.5 mm (P1), 10 mm (P2), and 9.5 mm (P3), corresponding to improvements of 8.7%, 13%, and 17.4%, respectively. Notably, while larger HEA profiles consistently result in reduced settlement across all configurations, the effectiveness of the connectors demonstrates diminishing returns as the profile size increases. The HEA 100 profile exhibits the greatest variation in settlement based on connector position, suggesting that optimizing connector positions provides a more substantial advantage for smaller profile sizes.

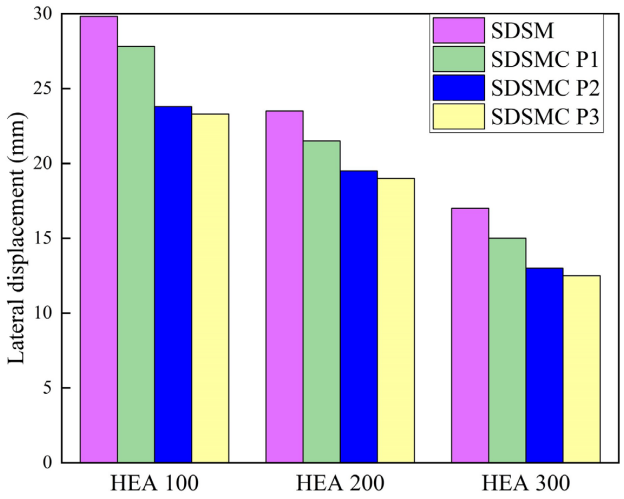

Figure 13. Maximum lateral displacement of SDSM and SDSMC walls with different HEA profile sizes (100, 200, and 300) and connector positions (P1, P2, and P3).

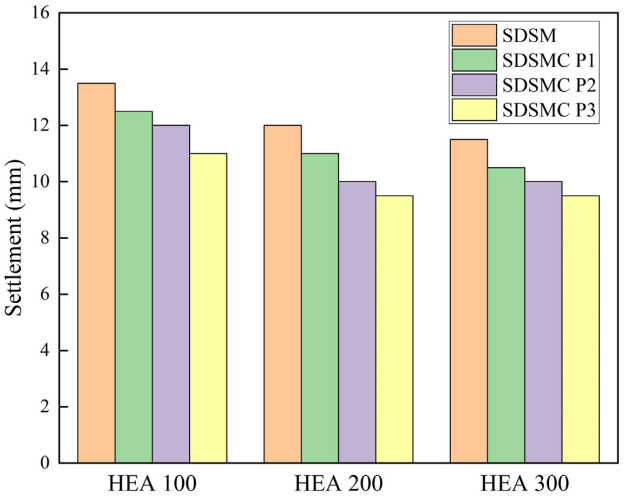

Figure 14. Maximum settlement of SDSM and SDSMC walls with different HEA profile sizes (100, 200, and 300) and connector positions (P1, P2, and P3).

5. Conclusion

This study investigates the performance of Stiffened Deep Soil Mixing (SDSM) walls with Connectors (SDSMC) in deep excavations. A finite element model, implemented in PLAXIS 3D, was used to numerically analyze the lateral displacements of the retaining walls and the ground surface settlement behind the walls. The comprehensive analysis of SDSMC walls reveals several key findings with significant implications for deep excavation applications in soft clay conditions.

- SDSMC walls significantly outperform conventional deep soil mixing walls, reducing lateral displacement and ground settlement;
- HEA profiles oriented perpendicular to the lateral earth pressure direction prove to be the most effective configuration, although differences between orientations remain relatively modest due to the uniform thickness characteristics of HEA profiles. The maximum displacement reduction of 66% was achieved under optimal conditions using the HEA300 section with X-direction orientation;
- The strategic deployment of two connectors at the top and bottom of the steel column resulted in wall performance enhancements of up to 30%. The strategic deployment of two connectors at the top and bottom of the steel column resulted in wall performance enhancements of up to 30%;
- The impact of connectors is more pronounced in smaller profiles (e.g., HEA 100) and diminishes as the profile size increases;
- The relationship between profile size and performance is non-linear, with the most significant improvements observed during the transition from HEA 100 to HEA 200;
- Two connectors are sufficient to achieve optimal performance, with minimal additional benefit gained from incorporating a third connector;
- The study suggests that a hybrid approach, using diverse HEA steel profiles with different section sizes (HEA100, HEA200, and HEA300) along the wall height, could enhance cost-effectiveness;
- For smaller steel profiles size, strategic connector positioning offers a cost-effective alternative to increasing the profile size.

However, these findings must be interpreted within significant study limitations. The practical applicability is limited to deep excavations in soft, highly compressible clay under similar modeled conditions. Extrapolation to other scenarios requires caution and additional validation through field studies. Future research should prioritize experimental validation of the SDSMC system, investigation of different column configurations, incorporation of time-dependent effects, and real project calibration. Economic feasibility studies and construction sequencing considerations would enhance practical engineering value.

Declaration of interest

The authors have no conflicts of interest to declare. All co-authors have observed and affirmed the contents of the paper and there is no financial interest to report.

Authors' contributions

Amira Aissaoui: data curation, visualization, writing – original draft, software. Rafik Boufarh: conceptualization, data curation, methodology, supervision, validation, writing – original draft, project administration. Farid Boursas: discussion of results, validation, writing – review & editing. Adel Djellali: supervision, validation, writing – review & editing.

Data availability

The datasets generated during and/or analyzed during the current study are available from the corresponding author on reasonable request.

Declaration of use of generative artificial intelligence

No generative artificial intelligence (GenAI) assistance tools were used in writing this paper.

List of symbols and abbreviations

c'	Cohesion
e_0	Initial void ratio
k	Swelling index
k^*	Modified swelling index
m	Power of the stress-level dependency of the stiffness
DSM	Deep Soil Mixing
E	Soil stiffness
E_{oed}^{ref}	reference oedometric modulus
E_{ref}	Reference stiffness at a σ_{ref}
E_{ur}^{ref}	Unloading/reloading stiffness of the soil
E_{50}^{ref}	Secant stiffness in triaxial tension at 50%
HEA	H-beam European standard, series A
HS	Hardening Soil constitutive model
I	Moment of Inertia
SDSM	Stiffened Deep Soil Mixing
SDSMC	Stiffened Deep Soil Mixing with connectors
γ	Unit weight
λ	Compression index
λ^*	Modified compression index
μ	Creep index
μ^*	Modified creep index
σ_{ref}	Reference stress
σ_3'	Current confining stress
v_{ur}	Poisson's ratio for elastic deformations
φ'	Friction angle

References

Andromalos, K.B., & Bahner, E.W. (2003). The application of various deep mixing methods for excavation support systems. In *Proceedings of the 3rd International Conference on Grouting and Ground Treatment*, New Orleans, LA, USA (pp. 515-526). Reston, VA: ASCE.

Bouassida, M., Fattah, M.Y., & Mezni, N. (2022). Bearing capacity of foundation on soil reinforced by deep mixing columns. *Geomechanics and Geoengineering*, *17*(1), 309-320. http://doi.org/10.1080/17486025.2020.1755458.

Bozkurt, S., Abed, A., & Karstunen, M. (2023). Finite element analysis for a deep excavation in soft clay supported by lime-cement columns. *Computers and Geotechnics*, *162*, 105687. http://doi.org/10.1016/j.compgeo.2023.105687.

Brinkgreve, R. (2004). Time-dependent behaviour of soft soils during embankment construction: a numerical study. In *Proceedings of the 9th International Symposium on'Numerical Models in Geomechanics* (pp. 631-637), Ottawa, Canada. London: CRC Press.

Bruce, D.A. (2000). *An introduction to the deep soil mixing methods as used in geotechnical applications.* Washington, D.C.: Office of Infrastructure, Federal Highway Administration.

Chen, J.-J., Zhang, L., Zhang, J.-F., Zhu, Y.-F., & Wang, J.-H. (2013). Field tests, modification, and application of deep soil mixing method in soft clay. *Journal of Geotechnical and Geoenvironmental Engineering*, *139*(1), 24-34. http://doi.org/10.1061/(ASCE)GT.1943-5606.0000746.

Do, T.-N., Ou, C.-Y., & Chen, R.-P. (2016). A study of failure mechanisms of deep excavations in soft clay using the finite element method. *Computers and Geotechnics*, *73*, 153-163. http://doi.org/10.1016/j.compgeo.2015.12.009.

Gupta, S., & Kumar, S. (2023). A state-of-the-art review of the deep soil mixing technique for ground improvement. *Innovative Infrastructure Solutions*, 8(4), 129. http://doi.org/10.1007/s41062-023-01098-6.

Hessouh, J.J., Eslami, J., Beaucour, A.-L., Noumowe, A., Mathieu, F., & Gotteland, P. (2023). Physical and mechanical characterization of deep soil mixing (DSM) materials: laboratory vs construction site. *Construction & Building Materials*, *368*, 130436. http://doi.org/10.1016/j.conbuildmat.2023.130436.

Jamsawang, P., Yoobanpot, N., Thanasisathit, N., Voottipruex, P., & Jongpradist, P. (2016). Three-dimensional numerical analysis of a DCM column-supported highway embankment. *Computers and Geotechnics*, *72*, 42-56. http://doi.org/10.1016/j.compgeo.2015.11.006.

Liu, G.B., Jiang, R.J., Ng, C.W., & Hong, Y. (2011). Deformation characteristics of a 38 m deep excavation in soft clay. *Canadian Geotechnical Journal*, *48*(12), 1817-1828. http://doi.org/10.1139/t11-075.

López Ramírez, A., Zhang, Y., Forsman, J., & Korkiala-Tanttu, L. (2024). Stabilization of soft clay with sustainable binders for dry deep mixing design. *Geotechnical Testing Journal*, *47*(1), 314-335. http://doi.org/10.1520/GTJ20220255.

Mun, B., Kim, T., Moon, T., & Oh, J. (2012). SCM wall in sand: numerical simulation and design implications. *Engineering Geology*, *151*, 15-23. http://doi.org/10.1016/j.enggeo.2012.09.003.

Navin, M. P. (2005). *Stability of embankments founded on soft soil improved with deep-mixing-method columns* [Doctoral thesis]. Virginia Polytechnic Institute and State University.

Ou, C.-Y. (2014). *Deep excavation: theory and practice*. London: CRC Press.

Phutthananon, C., Jongpradist, P., Kandavorawong, K., Dias, D., Guo, X., & Jamsawang, P. (2023). Reliability assessment for serviceability limit states of stiffened deep cement mixing column-supported embankments. *Journal of Rock Mechanics and Geotechnical Engineering*, *15*(9), 2402-2422. http://doi.org/10.1016/j.jrmge.2023.05.008.

Raongjant, W., & Jing, M. (2013). Field testing of stiffened deep cement mixing piles under lateral cyclic loading. *Earthquake Engineering and Engineering Vibration*, *12*(2), 261-265. http://doi.org/10.1007/s11803-013-0169-x.

Schanz, T., Vermeer, P., & Bonnier, P.G. (2019). The hardening soil model: formulation and verification. In R.B.J. Brinkgreve (Ed.), *Beyond 2000 in computational geotechnics* (pp. 281-296). London: Routledge.

Su, S., Liao, H., & Lin, Y. (1998). Base stability of deep excavation in anisotropic soft clay. *Journal of Geotechnical and Geoenvironmental Engineering*, 124(9), 809-819. http://doi.org/10.1061/(ASCE)1090-0241(1998)124:9(809).

Topolnicki, M. (2004). In situ soil mixing. In K. Kirsch & A. Bell (Eds.), *Ground improvement* (pp 331-428). New York: Taylor & Francis.

Vermeer, P., & Neher, H. (1999). A soft soil model that accounts for creep. In R.B.J. Brinkgreve (Ed.), *Beyond 2000 in computational geotechnics* (pp. 249-261). London: Routledge.

Voottipruex, P., Bergado, D., Suksawat, T., Jamsawang, P., & Cheang, W. (2011). Behavior and simulation of deep cement mixing (DCM) and stiffened deep cement mixing (SDCM) piles under full scale loading. *Soil and Foundation*, *51*(2), 307-320. http://doi.org/10.3208/sandf.51.307.

Voottipruex, P., Jamsawang, P., Sukontasukkul, P., Jongpradist, P., Horpibulsuk, S., & Chindaprasirt, P. (2019). Performances of SDCM and DCM walls under deep excavation in soft clay: field tests and 3D simulations. *Soil and Foundation*, 59(6), 1728-1739. http://doi.org/10.1016/j.sandf.2019.07.012.

Waichita, S., Jongpradist, P., & Jamsawang, P. (2019). Characterization of deep cement mixing wall behavior using wall-to-excavation shape factor. *Tunnelling and Underground Space Technology*, *83*, 243-253. http://doi.org/10.1016/j.tust.2018.09.033.

Wang, J., Xu, Z., & Wang, W. (2010). Wall and ground movements due to deep excavations in Shanghai soft soils. *Journal of Geotechnical and Geoenvironmental Engineering*, *136*(7), 985-994. http://doi.org/10.1061/(ASCE)GT.1943-5606.0000299.

Wonglert, A., Jongpradist, P., Jamsawang, P., & Larsson, S. (2018). Bearing capacity and failure behaviors of floating stiffened deep cement mixing columns under axial load. *Soil and Foundation*, *58*(2), 446-461. http://doi.org/10.1016/j.sandf.2018.02.012.

Yan, N., Li, G., Qin, F., Qiao, X., Lu, B., Liang, N., & Zhao, S. (2025). Study on the deformation characteristics of diaphragm walls in deep excavations within the Ningbo soft soil region. *Scientific Reports*, *15*(1), 15036. http://doi.org/10.1038/s41598-025-95878-y.

Zhang, Z., Rao, F.-R., & Ye, G.-B. (2020). Design method for calculating settlement of stiffened deep mixed column-supported embankment over soft clay. *Acta Geotechnica*, *15*(4), 795-814. http://doi.org/10.1007/s11440-019-00780-3.